mmWave Channel Propagation Modeling for V2X Communication Systems

Bogdan Antonescu
ECE Department
Northeastern University
Email: antonescu.b@husky.neu.edu

Miead Tehrani Moayyed
ECE Department
Northeastern University
Email: tehranimoayyed.m@husky.neu.edu

Stefano Basagni
ECE Department
Northeastern University
Email: basagni@ece.neu.edu

***Abstract*—We make the connection between next generation wireless standards (5G) and vehicular communication systems. We advocate the importance of transmissions in the millimeter wave band as the only ones capable to provide the Gbit/s data rates required for raw sensor data exchange among vehicles. In this context, our paper describes methods for deriving channel propagation models via ray-tracing simulations for mmWave transmissions with applications to vehicle-to-everything (V2X) communications. It also addresses aspects related to blockage modeling, the effects of diffuse scattering and multipath fading in urban scenarios.**

I. Introduction

The demand for capacity in mobile broadband communications shows a forecast for up to a thousand-fold increase in total traffic by 2020 [1]. The next generation (5G) wireless standard is looking into ways to solve the bandwidth bottleneck and to support these numbers together with other unique features like ubiquitous connectivity, very low latency, and high-speed data transfers. Options to achieve these goals include spectrum efficiency, spectrum extension and network densification. One of the many disruptive technologies of future wireless networks is *millimeter-wave* (mmWave), a promising candidate for *spectral extension* with multiple GHz of unused bandwidth in the 30–300 GHz range.

A great deal of research has focused on many mmWave frequency bands (e.g., 28 GHz, 38 GHz, 60 GHz, 71–76 GHz, 81–86 GHz). Standards, including IEEE 802.15.3c, 802.11ad, have been developed for indoor Wireless Personal Area Networks (WPNA) and Wireless Local Area Networks (WLAN). Unfortunately, there are many differences between mmWave communications and existing sub-6 GHz communication systems (e.g., high propagation loss, directivity, and sensitivity to blockage), so implementing transmissions in these extremely high frequency bands brings in new challenges [2], [3]. These are related to range and directional transmissions, shadowing, fading due to atmospheric conditions, rapid channel fluctuations due to mobility, and multiuser coordination to increase spatial reuse and spectral efficiency.

978-1-5386-3531-5/17/$31.00

In this paper we are concerned with the usage of mmWave frequencies for automotive applications, and in particular with the task of generating an accurate *radio channel propagation model* for vehicular (V2X) transmissions, which include vehicle-to-vehicle (V2V) and vehicle-to-infrastructure (V2I) communications. These applications are paramount to the future of transportation, and range from *autonomous driving* to *vehicle safety*, which have been at the core of automotive communications for a long time [4]. Predictions for future autonomous vehicles foresee up to 1 TB of generated data per driving hour, with rates achieving more than 750 Mbit/s [5]. This proves the limitations of current wireless technologies for exchanging automotive data, and justifies the use of the mmWave spectrum for increased data capacity and decreased latency because of the much larger bandwidth allocations. In addition to that, non-line-of-sight (NLOS) transmissions are a great challenge for mmWave communications and, at the same time, an enabler of the *fully connected vehicles* concept [6] that would allow cars to implement more powerful real-time safety applications, like "See Through" and "Bird's Eye View" [7].

Our investigation focuses on the NLOS key element through extensive simulations of path loss and network coverage when communications suffer from blockage due to obstacles, buildings and other cars. Through the proposed channel modeling and analysis, we also focus on other important design aspects of mmWave vehicular networks related to *directionality* of transmissions and the effect of various *beamwidths*.

The rest of the paper is organized as follows. Section II describes briefly various methods for deriving channel propagation models, and argues in favor of using ray-tracing simulation techniques. Section III tackles the problem of blockage for mmWave transmissions in an urban scenario. Section IV provides insights about multipath fading and the effects of diffuse scattering. Section V draws the conclusions regarding the usefulness of ray-tracing simulations for deriving channel propagation models for mmWave communications, and offers few possible ideas for future research.

II. Channel Propagation Modeling

Evaluating the performance of mmWave networks requires suitable *radio channel models* that can be obtained either through extensive measurements performed with steerable antennas and channel sounders, or via software ray-tracing simulators.

Measurement campaigns are time consuming, and require dedicated hardware (e.g., directive antennas) and very expensive test equipment (e.g., vector network analyzers, channel sounders). Nevertheless, a great deal of research and measurements were performed on mmWave propagation, covering many of the bands in this spectrum. To give only few examples, the 60 GHz band was the subject of [8], [9], [10]. Other channel measurements have been performed in the 28 GHz [11], [12] and the 38 GHz bands [13], [14], [15], as well as in the 73 GHz band [16], [17]. These studies were concerned with many aspects of large-scale and small-scale propagation effects (e.g., path loss exponent, maximum coverage and outage, penetration and reflection losses, angle of departure/arrival, multipath effects).

We chose the other option and we selected a software ray-tracing simulator, a professional tool (Wireless InSite) designed by Remcom. The advantage of a ray-tracer is the independence in choosing any indoor or outdoor scenario and in making the results valid for a wide range of use-case scenarios that have great similarity with the simulated one. The only important requirement is to build or import (in the ray-tracer) a very accurate description of all elements part of the application setting, so the simulation environment resembles the reality with a high degree of confidence. Thus, a customer who takes our channel propagation models (for specific streets of a certain city) can adapt them easily to another urban scenario. If the new scenario is fairly similar to ours, then all our results apply directly. If the new topography has major changes, then the simulation techniques still apply, but the results will be slightly different. The point is that making changes in the simulation environment and importing a new layout, or even creating a new one is still cheaper and faster than performing an extensive measurement campaign for a new site. There is no doubt that in the end these simulations can be followed by measurements, to verify the proposed channel model, but, as a first step, the ray-tracer provides a relatively quick methodology to estimate the hurdles in designing a mmWave network for a specific use-case scenario.

A. Channel propagation concepts

In a radio channel, the received power is affected by attenuation characterized by a combination of three main effects: Path loss, shadowing loss and fading loss. The first two are important for characterizing the *large-scale* propagation model of the radio channel. The third one is mainly addressed in connection with the *small-scale* propagation model. *Path loss* is the signal attenuation due to a decreased antenna reception when the distance between Tx and Rx increases; it is associated with a path loss exponent n that shows how fast path loss increases in various environments. Equally important for the large-scale propagation model is the *shadowing loss* caused by the absorption of the radiated signal by obstacles and scattering structures. The shadowing factor χ_σ is part of the path loss equation (1) and is typically modeled by a random variable with log-normal distribution with zero mean and standard deviation σ:

$$PL(d)[dB] = PL_{FS}(d_0) + 10nlog_{10}\frac{d}{d_0} + \chi_\sigma \quad (1)$$

where $PL(d_0)$ is the free-space loss at reference distance d_0 given by: $PL_{FS}(d_0)[dB] = 20log_{10}\frac{4\pi d_0}{\lambda}$. Other models for Equation 1 have been proposed in research literature ([18], [19]), but this is one of the most successful ones that covers a wide range of distances with great accuracy. The goal of all studies and measurements related to producing large-scale channel propagation models is in estimating the path loss exponent n and the shadowing factor χ_σ (i.e., its standard deviation σ that shows how much the instantaneous path loss varies from the average value). Measurement campaigns extract the statistics for both values from the captured data set. Our ray-tracer provides the path loss values for the specific use-case scenario (together with many other parameters of the radio channel), and using Matlab, we estimate n and σ. In the end, we compare the path loss plot obtained through curve fitting with the one produced by Equation 1 in which we plug the estimated values.

If we do not have a LOS between Tx and Rx, then the radio waves arrive at the receiver from different directions and with different propagation delays after *reflection*, *diffraction* and *scattering*. These *multipath* components with randomly distributed amplitudes, phases and angles-of-arrival (AoAs), combine at the Rx causing the received signal to distort or fade. Besides multipath, other factor that influences the small-scale propagation channel model is the *Doppler spread* due to mobility and speed of Tx and Rx (represented by cars, people and other moving objects). In a nutshell, the *small-scale effects* are considered rapid changes of the received signal strength over a *small* travel distance or time interval, random frequency modulation due to Doppler shifts, and time dispersion caused by multipath propagation delays. In a mobile radio channel, the type of fading that a signal experiences is provided by the relationship between the signal parameters (bandwidth, symbol period) and the channel parameters (Doppler spread/Coherence time and Delay spread/Coherence bandwidth). Thus, the small-scale fading due to multipath delay spread and the small-scale fading due to Doppler spread create four different types of fading by combining flat or frequency selective fading with fast or slow fading.

Fig. 1. Urban V2I scenario: LOS and NLOS reception.

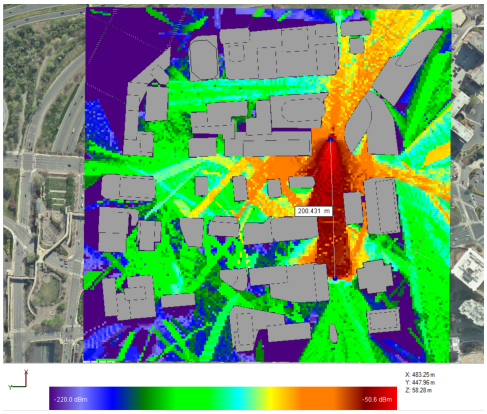

Fig. 2. Power coverage with 22° horn antennas: V2I scenario.

Our analysis follows a two-path approach. The first one approaches the large-scale channel propagation model for which we generate path loss and shadowing models. The second one tackles the small-scale channel propagation model in which we investigate multipath delay spread.

III. Blockage Modeling

In this section we simulated the 28 GHz transmission between transmitter and receiver units in both LOS and NLOS, using one of the urban scenarios (Rosslyn, VA) delivered with the ray-tracing tool. The Tx (base station) was located at a fixed site on a light/traffic pole (with a height of 10 m) in the North part of Fig. 1, and the Rx point was installed in a vehicle at approximately 1.5 m above ground. By placing the vehicle along the North-South wide-open boulevard at different locations up to 150 m in front of the transmitter, we simulated the LOS transmission. By moving the vehicle at distances 70 to 150 m from Tx, on a side street behind very tall buildings (East-West orientation in Fig. 1), we simulated the NLOS reception mode and the *effect of blocking*. Through the GUI of the ray-tracer, we selected two horn antenna models with different half-power beamwidth (HPBW) and gain (7°/25 dBi and 22°/15 dBi). In all simulations described in this paper, the same antennas were used at both Tx and Rx locations. The maximum power of the transmitted signal was set to 24 dBm. We also chose the number of reflections (6) and diffractions (1) that are used while tracing rays from transmitter to receiver. The coverage map (i.e., received power level) for 22°/15 dBi horn antennas is shown in Fig. 2.

We estimated the *path loss exponent* (n) and the standard deviation (σ) of the *shadowing factor* by placing randomly the receiver and recording 50–100 path loss values at each location for both LOS and NLOS. As expected, the results showed increased values for both parameters (n and σ) in the NLOS case comparing with the LOS case. They were in accordance with measurement campaigns for other urban scenarios [15], [1]. We applied the minimum mean square error (MMSE) method to the path loss values estimated by the ray-tracer, to extract n and σ. Using these values, we plotted the *path loss close-in* (PLCI) model given by Equation (1). We also considered another method to extract the statistics and to plot the path loss; this *floating intercept* model is also known as *alpha plus beta* model. We have to emphasize that the floating intercept model has no physical basis outside the studied distance range. Even though the fitted curve for the floating intercept matches the PLCI model for the analyzed Tx-Rx separation, only the PLCI model makes sense outside this range since it refers to an anchor point (i.e., the path loss at the 1 m reference distance).

While extracting the path loss statistics, we analyzed the influence of *beam alignment* and *beamwidth*. The former means that we apply a *continuous beam alignment* technique between Tx and Rx antennas based on detecting the path with the best received power value at each random Rx position. The latter implies a comparison between the two horn antennas (7°/25 dBi and 22°/15 dBi). For the more interesting NLOS case, path loss becomes much bigger ($n = 4.71$) with distance for a 22° horn antenna (Fig. 3) when we do not implement the beam alignment versus when we apply this technique ($n = 2.71$). The case of the 7° horn antenna is even more dramatic (Fig. 4) since the path loss exponent is larger ($n = 6.20$) when Tx and Rx antennas are in a fixed orientation (along the streets) versus when they constantly align their beams ($n = 2.72$). The variation of the instantaneous path loss due to shadowing is more pronounced ($\sigma = 6.53$) when the beamwidth is narrower (7°) and no beam alignment is applied, comparing with the beam alignment case ($\sigma = 4.11$).

To realize the significance of beam alignment (Fig. 5), a narrower beam antenna performs worse (i.e., higher path loss) if there is no beam alignment because only a few reflected or scattered rays are captured. In contrast, when beam alignment is applied (Fig. 6), the difference between the 7° and the 22° horn antennas is barely noticeable. This means that aligning the beams of the Tx

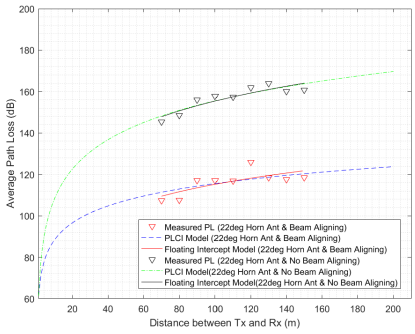

Fig. 3. Beam alignment effect on 22° horn antennas.

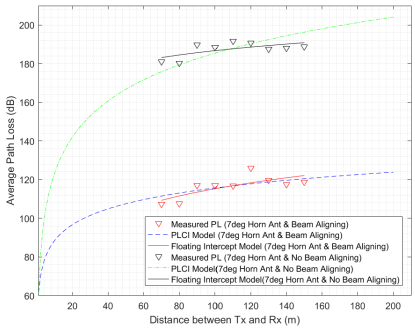

Fig. 4. Beam alignment effect on 7° horn antennas.

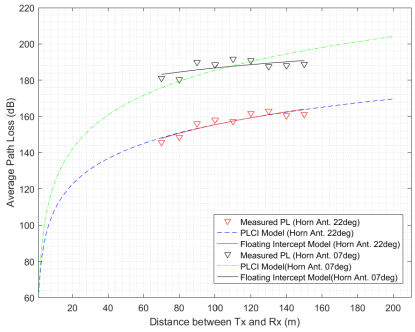

Fig. 5. Beamwidth effect *without* beam alignment: NLOS.

and Rx antennas is much more important than antenna beamwidth.

The LOS simulations confirmed path loss exponent values closer to the free space propagation ($n = 2$). The use of the 7° horn antenna with beam alignment resulted in a value of $n = 2.0048$ for this exponent, while the no beam alignment procedure increased it to $n = 2.67$. For the same scenarios, the 22° horn antenna generated similar values ($n = 2.0024$ with beam alignment and $n = 2.14$ without).

This section proved that the ray-tracing tool provides a fast way to obtain good path loss statistics and coverage maps in mmWave cells without the need for immediate

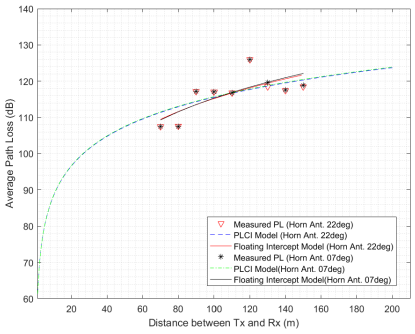

Fig. 6. Beamwidth effect *with* beam alignment: NLOS.

investigations and measurements in the field.

IV. Multipath Fading

For any wireless channel, one major concern is *multipath*, which corrupts the wanted signal by producing distortions and time-delayed copies of the transmitted signal.

To evaluate the channel time dispersive properties, we analyzed the *RMS delay spread* of the rays received at the Rx point (the static vehicle in the V2I scenario). The RMS value is similar to the standard deviation of a statistical distribution, and provides an indication about the severity of *Inter Symbol Interference* (ISI). As a rule of thumb, an RMS delay spread ten times smaller than the transmitted symbol time period guarantees no requirement for an ISI equalizer at the receiver. To overcome the multipath problem, in OFDM, a guard interval or cyclic prefix (CP) is attached at the beginning of the symbol (in time domain). This prevents ISI between consecutive OFDM symbols, as long as the typical delay spread of the channel is less than the guard interval. Once the CP value is known, it can be mapped to the estimated RMS delay spread obtained with a ray-tracer. To realize how RMS delay spread is affected by various transmission or simulation factors, we performed a series of experiments.

Beamforming and *directional transmissions* are two very important techniques used in mmWave communications to combat path loss. To prove the contribution of *directivity*, we used again the NLOS scenario from Section III. At each Tx-Rx separation distance, we used Matlab to generate 300 random points (i.e., Rx points) that were given to the ray-tracer for simulation. The result was a decrease of the RMS delay spread value when the antenna beamwidth changed from 22° to 7° (Fig. 7). The reduction in beamwidth implies an increase in gain (15 dBi vs. 25 dBi). We mention that the two simulations used the *beam alignment* mentioned in Section III. By doing that, we latched on the strongest received rays that dominated the delay spread, so the

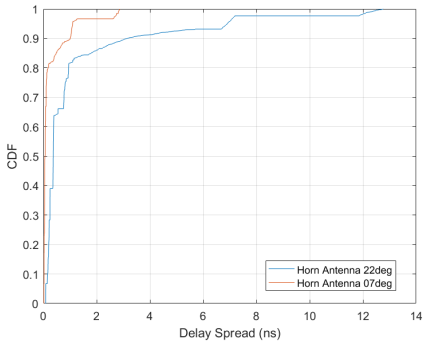

Fig. 7. Beamwidth effect in NLOS: Beam alignment.

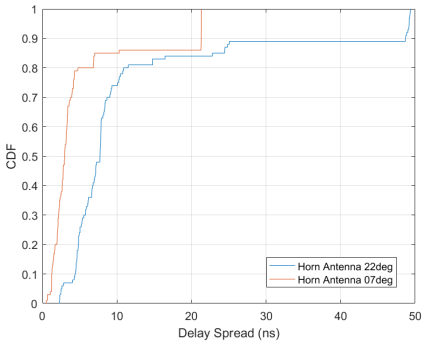

Fig. 9. Beamwidth effect at the cell edge: *With* beam alignment.

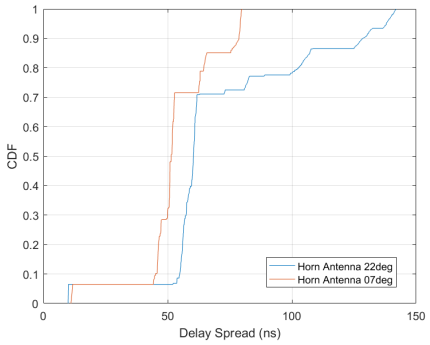

Fig. 8. Beamwidth effect at the cell edge: *Without* beam alignment.

result was smaller values for the RMS delay spread for both antenna beamwidths.

In another test, we moved towards the edge of the mmWave small-cell and we performed the same beamwidth study. This time, we chose only 50 random Rx points at each Tx-Rx separation distance (170, 180, 190, and 200 m), so the graphs were not as smooth as in the previous test that used 300 points at each distance. First, there was no beam alignment between Tx and Rx. That allowed the Rx to capture only the rays that entered its reception beam, not necessarily the strongest ones (Fig. 8). Then, we switched back to our beam alignment technique and checked for the strongest reception path (Fig. 9). The recorded RMS delay spread values showed two trends. An increase in the RMS delay spread values at the edge of the cell, even more visible when we didn't perform the beam alignment (Fig. 8). Second, the fact that narrow (7°) beamwidth antennas with more gain had smaller RMS delay spread values. The only time this last statement was not true in NLOS was when the Rx point was relatively close to the Tx point and the beam alignment was not applied. In that case, the narrow beam antenna missed the stronger multipath components comparing with the wider beam antenna, so its RMS delay spread was larger. The *beamwidth study* had two important results that confirmed the research performed by other teams with different tools or via direct measurements. One showed that beamwidth and directivity are crucial. The other one demonstrated that RMS delay spread could be a useful indicator in the process of designing mmWave directional systems based on beam searching algorithms.

In a second experiment, we emphasized the importance of *diffuse scattering*. Most of the available ray-tracers only account for rays that undergo specular reflections or diffractions, failing to describe diffuse scattering, which can have a significant impact in estimating accurately the channel dispersion, especially in T-shaped or X-shaped street intersections. Diffuse scattering refers to signals that are scattered in many directions, including the usual specular direction. These signals are generated because of gaps and sharp changes in the walls of a building that destroy its flat layer (e.g., windows, balconies, brick or stone decorations, beams). Last but not least, the type of material matters, creating an effective roughness for each wall.

The Wireless InSite ray-tracer offers the option of using three types of diffuse scattering models (Lambertian, directive, and directive with back scatter), to increase the multipath richness of the simulation. We chose Lambertian model that centers the scattering around the surface normal. We considered the same V2I static scenario at the edge of the small cell (i.e., Tx-Rx separation of 170, 180, 190, and 200 m) with NLOS reception mode. The simulation used 22°/15 dBi horn antennas with no alignment between the Tx and Rx antennas, and 100 random Rx points for each Tx-Rx separation distance. First, we ran the simulation without scattering. Then, we set the ray-tracer to include the effect of diffuse scattering. Plots of the cumulative distribution function (CDF) of the estimated RMS delay spread for these transmissions with and without scattering are presented in Fig. 10. While the mean excess delay increased when we considered diffuse scattering because we captured many more rays, the value of the RMS delay spread decreased because of the diffuse spread of power in all

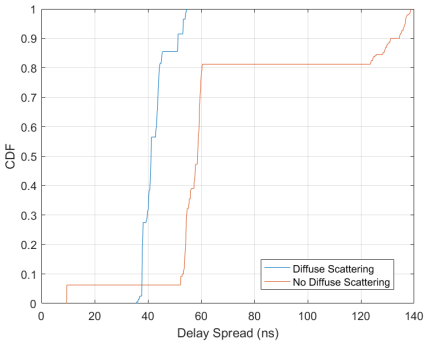

Fig. 10. Scattering effect on RMS delay spread in NLOS.

directions at the scattering objects that caused less power to be received at the receiver. More tests are required to study the effect of scattering with different antennas and different street intersections, together with a comparison of continuous beam alignment vs. no alignment, in the proximity of the transmitter as well as at distances close to the edge of the cell, and even outside this boundary.

V. Conclusions

This paper highlighted the bridge between the next generation 5G wireless networks and future vehicular communication systems. As mmWave will be one of the disruptive technologies part of these networks, we consider of utmost importance the research for an accurate radio channel propagation model in this frequency spectrum. Our paper introduced one such professional tool (Wireless InSite), and provided few examples for its usage in the study and generation of both large-scale and small-scale propagation models.

We plan to investigate mobility and the local-time varying nature of the radio channel through Doppler Spectrum and Coherence Time. This will allow us to provide comprehensive simulations of the mmWave channel in all types of vehicular communications, including the effect of mobile, large scatterers.

Acknowledgments

This work is supported in part by MathWorks under Research Grant "Cross-layer Approach to 5G: Models and Protocols." Particularly, we would like to thank Mike McLernon, Darel Linebarger and Paul Costa of MathWorks for their continued support and guidance on this project.

References

[1] Rappaport, T. et al., "Millimeter wave mobile communications for 5G cellular: It will work!" *IEEE Access*, vol. 1, pp. 335–349, May 2013.

[2] Y. Niu, Y. Li, D. Jin, L. Su, and A. V. Vasilakos, "A survey of millimeter wave communications (mmWave) for 5G: Opportunities and challenges," *Wireless Networks*, vol. 21, no. 8, pp. 2657–2676, April 2015.

[3] S. Rangan, T. S. Rappaport, and E. Erkip, "Millimeter-wave cellular wireless networks: Potentials and challenges," *Proceedings of the IEEE*, vol. 102, no. 3, pp. 366–385, March 2014.

[4] S. Tsugawa, "Issues and recent trends in vehicle safety communication systems," *Proceedings of IATSS Research*, vol. 29, no. 1, pp. 7–15, 2005.

[5] C. Perfecto, J. Del Ser, and M. Bennis, "Millimeter wave V2V communications: Distributed association and beam alignment," *IEEE Journal on Selected Areas in Communications*, no. 99, June 2017.

[6] J. Choi, V. Va, N. Gonzalez-Prelcic, R. Daniels, C. R. Bhat, and R. W. Heath Jr., "Millimeter-wave vehicular communication to support massive automotive sensing," *IEEE Communications Magazine*, vol. 54, no. 12, pp. 160–167, December 2016.

[7] "5G automotive vision," https://5g-ppp.eu/wp-content/uploads/2014/02/5GPPP-White-Paper-on-Automotive-Vertical-Sectors.pdf, 2015.

[8] T. S. Rappaport, J. N. Murdock, and F. Gutierrez, "State of the art in 60-GHz integrated circuits and systems for wireless communications," *Proceedings of the IEEE*, vol. 99, no. 8, pp. 1390–1436, August 2011.

[9] R. Daniels, J. Murdock, T. S. Rappaport, and R. W. Heath Jr., "60 GHz wireless: Up close and personal," *IEEE Microwave Magazine*, vol. 11, no. 7, pp. 44–50, December 2010.

[10] C. R. Anderson and T. S. Rappaport, "In-building wideband partition loss measurements at 2.5 and 60 GHz," *IEEE Transactions on Wireless Communications*, vol. 3, no. 3, pp. 922–928, May 2004.

[11] Zhao, H. et al., "28 GHz millimeter wave cellular communication measurements for reflection and penetration loss in and around buildings in New York City," in *Proceedings of IEEE ICC 2013*, Budapest, Hungary, June 9–13 2013.

[12] Samimi, M. K. et al., "28 GHz angle of arrival and angle of departure analysis for outdoor cellular communications using steerable beam antennas in New York City," in *Proceedings of IEEE VTC Spring 2013*, Dresden, Germany, June 2–5 2013.

[13] J. N. Murdock, E. Ben-Dor, Y. Qiao, J. I. Tamir, and T. S. Rappaport, "A 38 GHz cellular outage study for an urban outdoor campus environment," in *Proceedings of IEEE WCNC 2012*, Shanghai, China, April 1–4 2012.

[14] T. S. Rappaport, E. Ben-Dor, J. N. Murdock, and Y. Qiao, "38 GHz and 60 GHz angle-dependent propagation for cellular & peer-to-peer wireless communications," in *Proceedings of IEEE ICC 2012*, Ottawa, ON, Canada, June 10–15 2012.

[15] Sulyman, A. I. et al., "Radio propagation path loss models for 5G cellular networks in the 28 GHz and 38 GHz millimeter-wave bands," *IEEE Communications Magazine*, vol. 52, no. 9, pp. 78–86, September 2014.

[16] G. R. MacCartney and T. S. Rappaport, "73 GHz millimeter wave propagation measurements for outdoor urban mobile and backhaul communications in New York City," in *Proceedings of IEEE ICC 2014*, Sydney, NSW, Australia, June 10–14 2014.

[17] H. C. Nguyen, G. R. MacCartney Jr., T. Thomas, T. S. Rappaport, B. Vejlgaard, and P. Mogensen, "Evaluation of empirical ray-tracing model for an urban outdoor scenario at 73 GHz E-band," in *Proceedings of IEEE VTC Fall 2014*, Vancouver, BC, Canada, September 14–17 2014.

[18] Sun, S. et al., "Investigation of prediction accuracy, sensitivity, and parameter stability of large-scale propagation path loss models for 5G wireless communications," *IEEE Transactions on Vehicular Technology*, vol. 65, no. 5, pp. 2843–2860, May 2016.

[19] G. R. MacCartney Jr., T. S. Rappaport, S. Sun, and S. Deng, "Indoor office wideband millimeter-wave propagation measurements and channel models at 28 and 73 GHz for ultra-dense 5G wireless networks," *IEEE Access*, vol. 3, pp. 2388–2424, October 2015.